Consistency of the growth rate in different environments with the 6-degree Field Galaxy Survey: Measurement of the void-galaxy and galaxy-galaxy correlation functions

I. Achitouv,[1,2,*] C. Blake,[1,2] P. Carter,[3] J. Koda,[4] and F. Beutler[3]

[1]*Centre for Astrophysics & Supercomputing, Swinburne University of Technology, P.O. Box 218, Hawthorn, VIC 3122, Australia*

[2]*ARC Centre of Excellence for All-sky Astrophysics (CAASTRO), Australia*

[3]*Institute of Cosmology & Gravitation, Dennis Sciama Building, University of Portsmouth, Portsmouth, PO1 3FX, United Kingdom*

[4]*Department of Mathematics and Physics, Universita Roma Tre, Via della Vasca Navale 84, Rome 00146, Italy*

(Received 13 June 2016; published 4 April 2017)

We present a new test of gravitational physics by comparing the growth rate of cosmic structure measured around voids with that measured around galaxies in the same large-scale structure data set: the low-redshift 6-degree Field Galaxy Survey. By fitting a redshift space distortion model to the two-dimensional galaxy-galaxy and void-galaxy correlation functions, we recover the growth rate values $f\sigma_8 = 0.42 \pm 0.06$ and 0.39 ± 0.11, respectively. The environmental dependence of cosmological statistics can potentially discriminate between modified-gravity scenarios which modulate the growth rate as a function of scale or environment and test the underlying assumptions of homogeneity and isotropy.

DOI: 10.1103/PhysRevD.95.083502

I. INTRODUCTION

Galaxy peculiar velocities are a powerful probe of gravitational physics. They are sourced by virialized motion within halos and the overall bulk-flow motions due to gravitational interactions, leading to the mass assembly of halos. Although direct measurement of galaxy peculiar velocities is challenging, their correlated effect is imprinted in the clustering of matter through redshift space distortion (RSD), allowing us to determine the linear growth rate of structure. This quantity describes the growth of matter perturbations through cosmic evolution and contains critical information on cosmic expansion and gravitational physics.

For standard general relativity, in homogeneous and isotropic cosmologies, the growth rate in linear perturbation theory does not depend on the comoving spatial scale [1] and can be approximated by $f \sim \Omega_m(z)^\gamma$ where Ω_m is the matter density parameter at redshift z, and γ is a constant. For a ΛCDM universe $\gamma \sim 0.55$, independently of scale and environment. This would not be the case for different cosmological scenarios. For instance, inhomogeneous models of dark energy can lead to patches of clustered dark energy (e.g. Refs. [2,3]) which will have different expansion histories, and certain models of modified gravity such as $f(R)$ [4] rely on the Chameleon effect [5] that suppresses the gravitational force in underdense environments. These theories would naturally lead to an environmentally dependent growth rate and possibly a breakdown of the cosmological isotropy of our Universe. As pointed out in Ref. [6], the scale on which the environment is defined is important. For very large underdense regions, the effective cosmological parameters are expected to be different than the global-averaged parameters, but the quantification of this critical scale can also serve as an interesting test for departures from Einstein gravity.

A simple test of this physics is to compare the growth rate around cosmic voids to that inferred from galaxy clustering. In fact, nonlinear dynamics are expected to be reduced in cosmic voids compared to galaxy clustering in overdense regions [7]. Hence cosmic voids can potentially provide powerful tests of cosmology, for instance using the integrated Sachs-Wolfe effect [8] (e.g. Ref. [9]), the Alcock-Paczynski test [10] (e.g. Ref. [11]) or the void abundance and density profile (e.g. Refs. [12–16]).

In this work we test the consistency of the growth rate with environment using RSD measurements around voids and galaxies in the *6-degree Field Galaxy Survey* (6dFGS) [17,18], a low-redshift large-scale structure data set. There are several advantages to performing these tests near $z = 0$. First, cosmic expansion is dominated by dark energy, and hence a measurement of the growth rate around cosmic voids is a particularly interesting test of dark energy clustering. Second, the impact of the Alcock-Paczynski effect at $z = 0$ is minimal, such that our measurements have little sensitivity to the assumed cosmology. Third, low-redshift surveys such as the 6dFGS have a much higher galaxy number density than high-redshift surveys, enabling a higher-resolution measurement of the density field. This is particularly important for identifying voids in an unbiased fashion. Finally, the 6dFGS also contains a set of direct galaxy

*iachitouv@swin.edu.au

peculiar velocity measurements derived using fundamental-plane distances [19]. Although we do not use these measurements in the present work, they offer interesting opportunities for future investigation.

The measurement of the growth rate using RSD in galaxy clustering has been previously investigated for many data sets including the 6dFGS [20], the 2dF Galaxy Redshift Survey (2dFGRS) [21–23], the Sloan Digital Sky Survey (SDSS) [24], the WiggleZ Dark Energy Survey [25], the Baryon Oscillation Spectroscopic Survey (BOSS) [26–28] and the VIMOS Public Extragalactic Redshift Survey (VIPERS) [29]. These measurements have shown a general consistency with the ΛCDM cosmological model, up to a 2.5% precision, albeit in some cases showing tension with the predictions of the latest cosmic microwave background measurements [30]. However, the measurement of the growth using RSD in void-galaxy clustering has not been widely investigated, although the authors of Refs. [7] and [31] recently reported measurements using the BOSS-CMASS sample and VIPERS, respectively. However, none of these studies has explored the consistency of the growth rate in different environments using the same galaxy survey.

This paper is organized as follows. In Sec. II we describe the model we use to fit the measurement of the galaxy-galaxy and void-galaxy correlation functions. In Sec. III we test these models using mock catalogues. In Sec. IV we apply our framework to the 6dFGS data and deduce constraints on the growth rate in different environments, and we conclude in Sec. V.

II. MODELS FOR THE TWO-DIMENSIONAL CORRELATION FUNCTIONS

The peculiar velocities of galaxies, $\mathbf{v}$, due to the local gravitational potential, result on small scales in random motions of galaxies within a group. By measuring galaxy positions in redshift space, we can observe the well-known "Finger-of-God" (FoG) effect. On large scales, the bulk flow (coherent infall/outflow in overdense/underdense regions) is responsible for an overall coherent distortion known as the "Kaiser effect" [32].

The mapping of the position of a galaxy from real space $\mathbf{r} = (x, y, z)$ to its position in redshift space $\mathbf{s}$ is given by

$$\mathbf{s} = \mathbf{r} + \frac{(1+z)v_p(\mathbf{r})}{H(z)}\mathbf{u_r}, \tag{1}$$

where $\mathbf{u_r}$ is the unitary vector along the line of sight, $v_p \equiv \mathbf{v}.\mathbf{u_r}$ and $H(z)$ is the Hubble parameter at redshift z. On large scales, where the matter overdensity grows coherently [32,33], linear perturbation theory implies that $\nabla.\mathbf{v} \propto -f\delta_m$ where δ_m is the matter density contrast and the linear growth rate of perturbations f is defined as

$$f \equiv \frac{d\ln\delta_m(a)}{d\ln a}. \tag{2}$$

We need to relate the observed galaxy overdensity, δ_g, to the matter density contrast, which we accomplish using a linear bias $b \equiv \delta_g/\delta_m$, which is independent of scale in the linear regime.

In what follows we use the notation σ for the component of galaxy-galaxy or void-galaxy separation perpendicular to the line of sight, and π for the component parallel to the line of sight. For both the galaxy-galaxy and the void-galaxy correlation functions, the random small-scale component of the peculiar velocity can be described by convolving the correlation function with a pairwise velocity distribution [1]. The latter is often modeled as a Gaussian or Lorentzian distribution; we consider both choices in our analysis.

A. The galaxy-galaxy correlation function

The redshift-space two-dimensional (2D) correlation function due to the coherent bulk flow of peculiar velocity can be described by [32,33]

$$\xi^l(\sigma,\pi) = \xi_0(s)P_0(\mu) + \xi_2(s)P_2(\mu) + \xi_4(s)P_4(\mu), \tag{3}$$

where $P_l(\mu)$ are Legendre polynomials and $\mu \equiv \cos(\theta)$ is the angle between the separation vector and line of sight. In the linear regime [32],

$$\xi_0(s) = \left(1 + \frac{2}{3}\beta + \frac{1}{5}\beta^2\right) \times b^2\xi(r),$$
$$\xi_2(s) = \left(\frac{4}{3}\beta + \frac{4}{7}\beta^2\right) \times b^2(\xi(r) - \bar{\xi}(r)),$$
$$\xi_4(s) = \frac{8}{35}\beta^2 \times b^2\left(\xi(r) + \frac{5}{2}\bar{\xi}(r) - \frac{7}{2}\bar{\bar{\xi}}(r)\right),$$

where $\beta = f/b$, the real-space matter correlation function is $\xi(r)$, and

$$\bar{\xi}(r) = (3/r^3)\int_0^r \xi(y)y^2dy,$$
$$\bar{\bar{\xi}}(r) = (5/r^5)\int_0^r \xi(y)y^4dy.$$

Including our model for small-scale random motions, the total 2D correlation function in redshift space is given by [1]

$$\xi_{gg}(\sigma,\pi) = \int \xi^l\left(\sigma, \pi - \frac{v}{H_0}\right)P(v)dv, \tag{4}$$

where $P(v)$ is the probability distribution of the random pairwise motions. In what follows we model the matter clustering using the nonlinear power spectrum from CAMB (halofit) [34] and Fourier transform it to obtain the nonlinear matter correlation function $\xi(r)$ in Eq. (4). We adopt a fiducial cosmology matching that of Mocks A described below: a flat WMAP 5-year cosmology [35] ($\Omega_m = 0.26$, $h = 0.72$, $\sigma_8 = 0.79$, $n_s = 0.963$, $\Omega_b = 0.044$).

B. The void-galaxy correlation function

The previous effects of the peculiar velocity also apply to the void-galaxy correlation function and we have [1]

$$\xi_{vg}(\sigma,\pi) = \int (1+\xi^{1D}_{vg}(y)) \times P\left(v - v_p(y)\left[\left(\pi - \frac{v}{H_0}\right)/y\right]\right) dv - 1, \quad (5)$$

where ξ^{1D}_{vg} is the angle-averaged void-galaxy correlation function in real space and $y = \sqrt{\sigma^2 + (\pi - v/H_0)^2}$.

We calibrate the model using the real-space void-matter cross-correlation $\xi_{v\text{-DM}}(r)$ measured from N-body simulations (see Sec. III) as our ΛCDM template, such that including the linear bias factor

$$\xi^{1D}_{vg}(r) = b\xi_{v-\mathrm{DM}}(r). \quad (6)$$

For coherent outflow motion, at linear order, the peculiar velocity can be expressed as [1]

$$v_p(r) = -\frac{1}{3} H_0 r \Delta(r) f, \quad (7)$$

where $\Delta(r)$ is the average integrated density contrast around voids. For spherical voids we have

$$\Delta(r) = \frac{3}{r^3}\int_0^r \xi_{v-\mathrm{DM}}(y) y^2 dy. \quad (8)$$

C. The pairwise velocity distribution

In this work we will consider two models G and L to describe the pairwise velocity distribution $P(v)$ in Eqs. (4) and (5): *model G* will use a Gaussian distribution given by

$$P(v) = \frac{1}{\sqrt{2\pi\sigma_v^2}} \exp\left[-\frac{v^2}{2\sigma_v^2}\right], \quad (9)$$

while *model L* will use a Lorentzian distribution (in Fourier space) which corresponds to convolution by an exponential distribution in configuration space

$$P(v) = \frac{1}{\sqrt{2\sigma_v^2}} \exp\left[-\frac{\sqrt{2}|v|}{\sigma_v}\right], \quad (10)$$

where σ_v is the standard deviation of the peculiar velocity. Our model hence neglects the scale dependence of σ_v [16,36,37].

A Gaussian distribution of peculiar velocities is often assumed for the random motions which result from halo relaxation. However, numerical studies (e.g. Ref. [38]) have shown that a Lorentzian distribution can provide a better empirical description of the distribution of peculiar velocities which might result from a superposition of different-mass haloes.

D. Summary of the variables

Our model hence consists of three parameters for both the galaxy-galaxy and void-galaxy correlation functions: the linear bias b which enters into Eqs. (3) and (6), the standard deviation of the peculiar velocity σ_v that enters into Eqs. (9) and (10), and the linear growth rate f that is part of Eqs. (3) and (7). We note that, in the linear-theory approximation, the fitted values of f and b are degenerate with the assumed normalization of the matter power spectrum, σ_8. We reflect this degeneracy by presenting our results in terms of the normalized variables $f\sigma_8$ and $b\sigma_8$.

E. Remarks on the models

The RSD models we use in our study, while commonly adopted in the literature, greatly simplify the nonlinear physics which will be present on these scales. For example, galaxy bias generally exhibits nonlinear, nonlocal, scale-dependent and stochastic properties [39] and the galaxy pairwise velocity dispersion may be scale dependent or non-Gaussian [16,36,37]. However, in the following section we will use mock catalogues to demonstrate that, at the level of statistical precision of the 6dFGS data set, these simple models are sufficient to extract unbiased estimates of the growth rate from both the galaxy-galaxy and void-galaxy correlations. Many studies have confirmed this conclusion through comparison with more sophisticated models (e.g. Ref. [20], in the context of 6dFGS). More accurate modeling of RSD is a significant challenge for upcoming galaxy surveys with much greater statistical precision such as Euclid [40].

III. TESTS ON MOCKS

In order to test our analysis pipeline and the limitations of our models, we measured the growth rate in two sets of mock catalogues. *Mocks A* are flat-sky mocks with no survey selection function applied, for which we possess the full set of dark matter and halo information. We used these mocks to model the extraction of galaxy voids from a volume-limited observational sample and the fitting of the void-galaxy correlation function. *Mocks B* are curved-sky mocks which incorporate the full 6dFGS selection function via detailed halo-occupation modeling. Although we do not have the dark matter information to allow tests of the void sample, we used these mocks to test the fitting of the galaxy-galaxy correlation function to the flux-limited observational sample. We summarize the creation of these two sets of mocks below.

A. Mocks A: Volume-limited samples

To generate Mocks A, we used a sample of dark matter particles and halos from the DEUSS simulations [41].

These simulations were run for several scientific purposes, as described in Refs. [42–44] and are freely available. The simulations were carried out using the RAMSES code [45] for a ΛCDM model calibrated to the WMAP 5-year cosmological parameters [35]. We used the $z = 0$ output of a simulation generated in a $648^3\ h^{-3}\,\mathrm{Mpc}^3$ box using 2048^3 particles.

In Sec. IV we will extract galaxy voids from a volume-limited sample of 6dFGS galaxies. We built a series of 20 dark matter ($b = 1$) catalogues approximately matching the number density and volume of this subsample, by randomly selecting $N_p = 15\,000$ DM particles a box of side length 140 h^{-1} Mpc. We also built 20 biased galaxy mocks by subsampling $N_h = 15000$ halos identified with the Friend-of-Friends algorithm with linking length 0.2, selecting the most massive haloes in order to approximately mimic the 6dFGS selection. Finally, in order to simulate the RSD we used the flat-sky approximation and shifted the positions of the DM particles and halos according to Eq. (1), using their peculiar velocities.

We note that, when generating these mocks, it is important to match the DM and halo number density to the galaxy data set in order to avoid introducing a bias in the identification of voids between the mock and the real data set. For instance, in Ref. [46], the authors showed that the density profile of voids is sensitive to the resolution of the simulation.

B. Mocks B: Selection-function samples

In Sec. IV we will use the magnitude-limited 6dFGS sample to measure RSD from the galaxy-galaxy correlations. We therefore supplemented Mocks A with a second simulation set, Mocks B, which provided a more accurate curved-sky modeling of the survey selection function and redshift dependence of the galaxy bias.

We built Mocks B from the COLA N-body simulations introduced in Ref. [47], using a modified version of the pipeline created by the authors of Ref. [48] to construct BOSS and WiggleZ mocks. In brief, we first fit the central and satellite galaxy halo occupation distribution of the 6dFGS galaxy sample as a function of luminosity [49]. By calibrating the luminosity-redshift relation, we defined the redshift evolution of the HOD. Through careful comparison of the projected and three-dimensional clustering of the mock and data sample, we iterated the HOD parameters to produce the closest possible match. We then applied peculiar velocities along the line of sight, and subsampled the resulting distribution with the 6dFGS angular selection function [50]. These mocks will be presented in more detail in Ref. [51].

C. Void-finding in Mocks A

In our analysis we identified voids with radius $R_v = 20\ h^{-1}$ Mpc using the void finder developed in Ref. [16]. This radius is chosen as a compromise between being small enough to obtain sufficient voids for an accurate measurement of the void-galaxy correlation function, but being large enough to select genuinely underdense patches of matter [52].

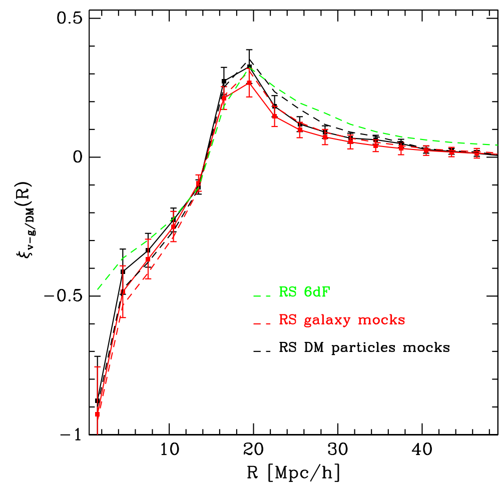

FIG. 1. Measurement of the one-dimensional void-DM and void-galaxy correlation functions. The error bars show the $1-\sigma$ standard deviation computed using the mock catalogues. The solid and dashed lines show measurements in real space and redshift space, respectively, for the DM particles (black lines), the haloes (red lines) and the 6dFGS galaxies (green line, only available in redshift space).

This void finder uses density criteria to identify voids with the characteristic profile illustrated in Fig. 1. For each of the candidate void positions, which are picked at random, the algorithm first requires that the overdensity δ is below a threshold in two central bins, $\delta(R_0) < \delta_1 = -0.9$ and $\delta(R_0 + \Delta R) < \delta_2 = -0.8$, where $R_0 = 0.5\ h^{-1}$ Mpc and $\Delta R = 1\ h^{-1}$ Mpc. The third condition ensures a ridge of the void profile by requiring that $\delta(R_v - \Delta R) < \delta(R_v)$ and the fourth condition controls the amplitude of the ridge by requiring that $\delta(R_v) > \delta_3 = 0$.

We used 10 times the number of candidate positions as tracers, producing a sample of ~300 voids for each Mock A, which is similar to the number density of voids we find by applying the same algorithm to the volume-limited 6dFGS subsample. We note that about half of these voids have some portion of overlap; this does not affect our analysis because overlap does not change the radial density profile [16], and any covariance between overlapping voids is already encoded in the measurement scatter between mocks.

D. One-dimensional matter-void cross-correlation function

We measured the void-tracer cross-correlation functions using the Landy-Szalay (LS) estimator:

$$\xi_{vg}(R) = \frac{N_{rg}N_{rv}}{R_v R_g}\left(\frac{D_v D_g}{N_g N_v} - \frac{D_g R_v}{N_g N_{rv}} - \frac{D_v R_g}{N_v N_{rg}}\right) + 1, \quad (11)$$

where $D_v D_g$ is the number of data void-galaxy pairs, $R_v R_g$ is the number of random void-galaxy pairs and $D_{g/v} R_{g/v}$ is the number of galaxy/void data-random pairs, in a bin at separation R. The total number of galaxies, voids, galaxy-randoms and voids-randoms are N_g, N_v, N_{rg} and N_{rv}, respectively. In all cases we generated random catalogues having 10 times the number of galaxies than our data samples.

The one-dimensional (1D) mock mean void-matter correlation function, $\xi_{v-\mathrm{DM}}(R)$, is displayed in Fig. 1 as the black data points. We also show the void-halo correlation function (red points), using voids identified in real-space mocks before applying RSD. In addition we compare the same measurements after RSD is applied (dashed lines), including the 6dFGS measurement. For clarity we do not show the errors in the redshift-space measurements, which are similar to the real-space case. We see that RSD accentuates the features of the void profile: it makes the inner density profile steeper and the ridge higher.

E. Model fits to the mock 2D correlation functions

We computed the 2D void-halo correlation function for Mocks A, and the halo-halo correlation functions for both Mocks A and B, using the LS estimator of Eq. (11). Indeed, it is interesting to also measure the galaxy-galaxy correlation in mocks A in order to (i) test if the inferred linear bias is the same as the one inferred from the galaxy-void measurement, and (ii) confirm that the inferred value of the growth rate is the same as the one inferred from the galaxy-void clustering. In fact, there should be a limit of the void size where nonlinear effects should impact the value of the growth rate inside large voids. Hence we checked that this effect does not occur for our selected voids by testing the consistency of the growth rate within the same mocks A. When measuring the correlation functions for Mocks B, which include the varying survey selection function, we used minimum variance weights [20,53]

$$w_i = \frac{1}{1 + n_i P_0}, \tag{12}$$

where (following Ref. [20]) $P_0 = 1600\ h^{-3}\,\mathrm{Mpc}^3$ and n_i is the galaxy number density at the location of the ith object. In Eq. (11), the ratio of random objects to data objects then becomes

$$\frac{N_{rg}}{N_g} \rightarrow \frac{\sum_{i=1}^{N_{rg}} w_i}{\sum_{j=1}^{N_g} w_j}. \tag{13}$$

We computed the 2D correlation functions of 20 mocks in (σ, π) bins of width 3 h^{-1} Mpc in the range 0–54 h^{-1} Mpc, and used these measurements to construct the standard deviation in each bin, σ_{mocks}.

For our first analysis we fitted the model to the *mock mean 2D correlation function*, with an error in each bin given by $\Delta\xi = \sigma_{\mathrm{mocks}}/\sqrt{N_{\mathrm{mocks}}}$. This allows us to perform precise systematic tests of Eqs. (4) and (5), using a mock data set with a statistical error far smaller than the real 6dFGS data set.

At small scales the galaxy-galaxy correlation function is dominated by the FoG effect, which cannot be described by the linear theory and pairwise velocity dispersion models of Eq. (4). Therefore, small σ bins are often excluded when computing the χ^2 [Eq. (14)]. For these reasons we apply a cut $\sigma_{\mathrm{cut}} > 7.5\ h^{-1}$ Mpc when fitting the galaxy-galaxy correlation function, while we keep all the separation bins for the void-galaxy correlation function. We consider below the sensitivity of our results to these choices.

We performed our fit using a Metropolis-Hastings Markov chain Monte Carlo (MCMC) analysis for the parameters $\Theta = (f\sigma_8, b\sigma_8, \sigma_v)$, analyzing our Monte Carlo chains using the module *GetDist* developed by Lewis [54]. We used priors $f\sigma_8 = [0.02, 0.71]$, $b\sigma_8 = [0.4, 1.58]$ and $\sigma_v = [25, 600]\ \mathrm{km\,s^{-1}}$, although our results are not sensitive to these choices. We computed the likelihood of each model assuming

$$\chi^2(\Theta) = \sum_{\sigma,\pi} \left[\frac{\xi^{\mathrm{data}}(\sigma,\pi) - \xi^{\mathrm{theo}}(\Theta,\sigma,\pi)}{\Delta\xi(\sigma,\pi)}\right]^2. \tag{14}$$

TABLE I. Parameter constraints obtained from fitting to the mock mean 2D galaxy-galaxy correlation function ξ_{gg} and void-galaxy correlation function ξ_{vg} for Mocks A and B, assuming Lorentzian (L) and Gaussian (G) models for the pairwise velocity dispersion. The reported parameter errors are the scatter in the fits to individual mocks, scaled by $\sqrt{N_{\mathrm{mocks}}}$. The χ^2 values are derived from the MCMC fit to the mock mean, which is impacted by neglecting off-diagonal covariance. The fiducial cosmology in the mocks is $f\sigma_8 = 0.26^{0.55} \times 0.79 \sim 0.38$.

	Mocks	$b\sigma_8$	σ_{IM}	$f\sigma_8$	σ_{IM}	$\sigma_v[\mathrm{km.s^{-1}}]$	σ_{IM}	$\chi^2/\mathrm{d.o.f}$
ξ_{gg} L	A	0.66	±0.02	0.37	±0.03	134	±21	497/192
ξ_{vg} L	A	0.67	±0.01	0.38	±0.02	126	±8.5	920/277
ξ_{gg} G	A	0.66	±0.02	0.37	±0.03	118	±19	497/192
ξ_{vg} G	A	0.67	±0.01	0.38	±0.02	122	±9	925/277
ξ_{gg} G	B	1.01	±0.01	0.38	±0.01	102	±21	327/192
ξ_{gg} L	B	1.00	±0.01	0.38	±0.01	100	±25	326/192

We cannot numerically determine the large covariance matrix between different (σ, π) bins sufficiently accurately to allow it to be inverted when determining the χ^2 statistic, so in Eq. (14) we assumed no correlation between bins. Our MCMC fit will therefore not produce robust parameter errors, and we instead used the dispersion of the best-fitting parameter values between individual mocks, σ_{IM}, as a more accurate estimate of the resulting errors. This scatter, which is typically double the parameter error obtained by the MCMC, naturally includes the effect of data correlations. When fitting to the mock mean, we report a scaled parameter error $\sigma_{IM}/\sqrt{N_{\mathrm{mocks}}}$.

We report the best-fitting parameter values and errors of our fits to the mock mean galaxy-galaxy and void-galaxy correlation functions, and minimum χ^2 values, in Table I. In Fig. 2, left panels, we show the mean measurement of the mock 2D void-galaxy and galaxy-galaxy correlation function. The solid lines correspond to the isocontour of our best fitting models. The right panels show the residual between the data and our models. We find that both the

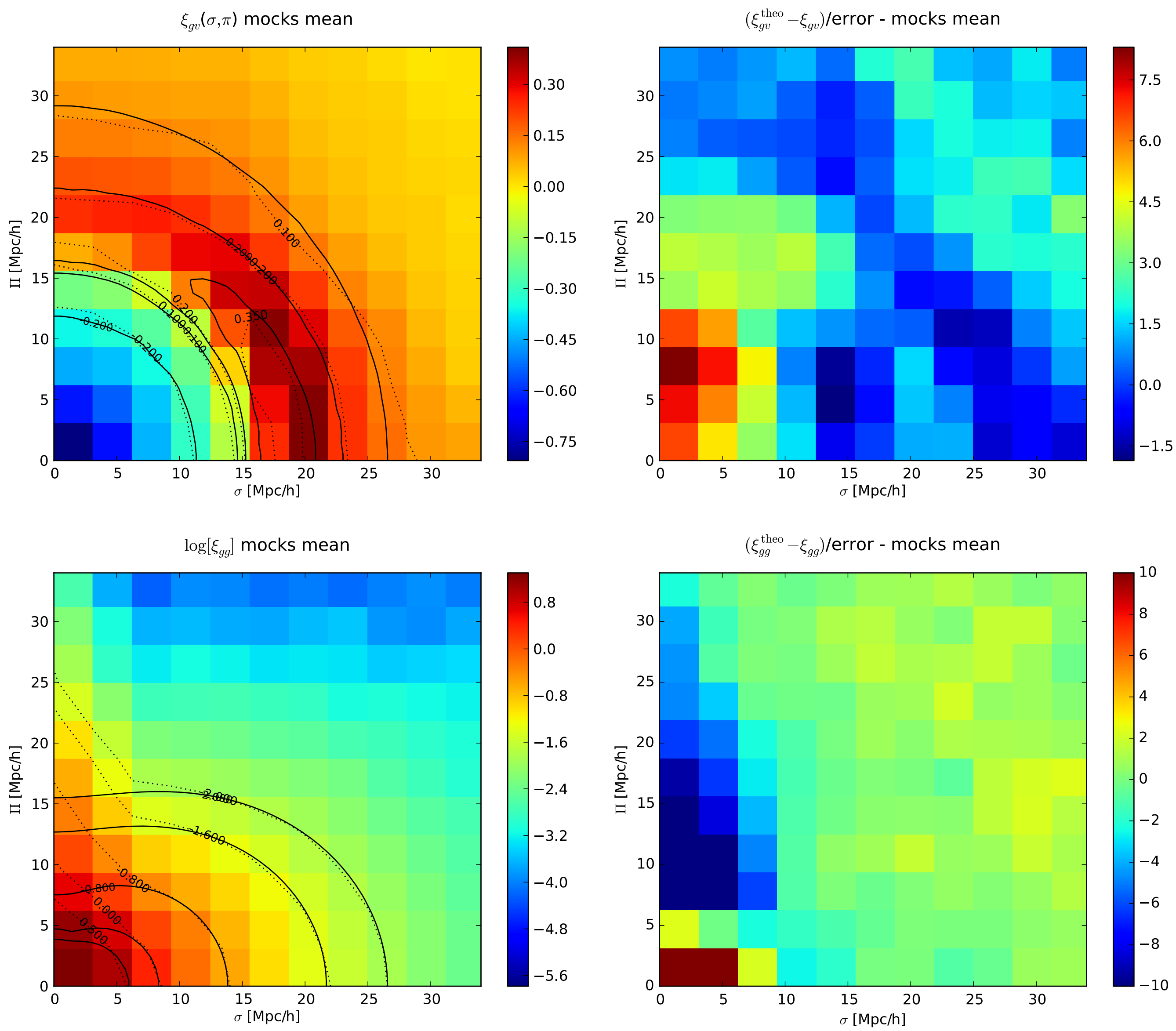

FIG. 2. The mean measurement of the mock 2D void-galaxy correlation function (upper-left panel) and galaxy-galaxy correlation function (lower-left panel). The solid lines show the best-fitting model assuming a Gaussian pairwise velocity distribution, and the dotted lines show isocontours of the data, noting that the fitting region for the galaxy-galaxy correlation function is $\sigma > 7.5\ h^{-1}$ Mpc. The right-hand panels show the residual between the measurements and best-fitting theory in each case, scaled by the standard deviation across the mocks. For the galaxy-galaxy residual we impose a min/max cut of $-10/+10$ in order to distinguish the variations across the right-hand side of the plot. We note that the mock mean is a substantially more accurate test of the model than a single data set, and some significant deviations from the model are detected. However, the resulting growth rate fits are unbiased.

Gaussian and the Lorentzian models lead to similar constraints on the growth rate, and that the best-fitting growth rates are consistent with the fiducial cosmology of the mocks ($f\sigma_8 = 0.26^{0.55} \times 0.79 \sim 0.38$), validating our models. The fits to Mocks A show that the fiducial growth rate is recovered around both voids and galaxies for a consistent tracer population, and that our choice of void size produces no unwanted systematic effect due to nonlinearity or inhomogeneity. The best-fitting χ^2 values are high for both statistics, although we note that these values neglect the off-diagonal elements of the covariance matrix, and that the mock mean provides a far more precise diagnostic of systematics than the real survey data.

The galaxy-galaxy RSD provides weaker constraints on σ_v than the void-galaxy correlation function, due to our exclusion of small σ scales from the fit in this case. The error in σ_v is sensitive to this cut, as we will see in Fig. 4. Table I also lists best-fitting values for the galaxy bias factor. We note that the galaxy bias factor for Mocks B is significantly higher than for Mocks A, because of the selection of more massive halos required to match the 6dFGS sample at higher redshifts, and the upweighting of those halos by the Feldman-Kaiser-Peacock weights. The comparison of the results of the void-galaxy and galaxy-galaxy correlation function fits for Mocks A allows us to verify that the measured tracer bias is consistent in the two cases, implying that there is not an environmental dependence of this parameter.

In Table II we report summary statistics of the fits of our model to the individual mock catalogues, listing the mean values of the best-fitting parameters ($\bar{f\sigma_8}$, $\bar{b\sigma_8}$, $\bar{\sigma_v}$) and their dispersion across the mock catalogues ($\sigma_{f\sigma_8}$, $\sigma_{b\sigma_8}$, σ_{σ_v}). The mean values are consistent with the best fit to the mock mean, indicating that our approach is unbiased.

We checked the dependence of the best-fitting parameter values on the range of scales included in our analysis. In the upper panel of Fig. 4, we show the variation of the best-fitting values with the cutting scale $\sigma_{\rm cut}$, for the fits to the galaxy-galaxy correlation function of Mocks B. The triangles (red for model G and orange for model L) show the result from fitting to the mock mean, while the unfilled circles correspond to the mean parameter fit to the individual mocks. The minimum reduced χ^2 is shown in the bottom panel. Deviations are seen when including the first bin, which we expect to be most strongly affected, although our results do not show a strong dependence on $\sigma_{\rm cut}$ and we adopt a baseline $\sigma_{\rm cut} = 7.5\ h^{-1}$ Mpc for our analyses.

A similar analysis of the void-galaxy correlation function of Mocks A is shown in the lower panel of Fig. 4 where, given the absence of nonlinear pairwise velocities, we now consider a cut as a function of the total separation, $R_{\rm cut} = \sqrt{\pi^2 + \sigma^2}$. This is motivated by the possibility that linear theory may break down at the center of the voids where $\delta_v(R \to 0) \approx -1$ [6]. We plot the best-fitting parameters as a function of $R_{\rm cut}$ as well as the reduced χ^2 for model G (blue lines) and model L (cyan lines). The fits to the mock mean are shown by the triangles, while the unfilled circles correspond to the mean parameter fit to the individual mocks. In this case, we find a low sensitivity of the results to the value of $R_{\rm cut}$. The best-fitting parameters are consistent with our fiducial cosmology when we use all scales ($R_{\rm cut} = 0$) in Eq. (14).

TABLE II. Parameter constraints obtained by fitting to each individual mock and measuring the resulting mean and standard deviation of the best-fitting parameters, for the 2D galaxy-galaxy correlation function ξ_{gg} and void-galaxy correlation function ξ_{vg}, assuming Lorentzian (L) and Gaussian (G) models for the pairwise velocity dispersion. The fiducial cosmology in the mocks is $f\sigma_8 = 0.26^{0.55} \times 0.79 \sim 0.38$.

	Mocks	$\bar{\sigma_8 b}/\sigma_{\sigma_8 b}$	$\bar{f\sigma_8}/\sigma_{f\sigma_8}$	$\bar{\sigma_v}/\sigma_{\sigma_v}$[km.s^{-1}]
ξ_{gg} L	A	0.58/0.20	0.36/0.24	293/166
ξ_{vg} L	A	0.70/0.08	0.44/0.18	164/68
ξ_{gg} G	A	0.58/0.19	0.38/0.29	270/150
ξ_{vg} G	A	0.70/0.08	0.42/0.19	181.5/72
ξ_{gg} G	B	1.0/0.06	0.39/0.06	111/92
ξ_{gg} L	B	1.0/0.06	0.39/0.06	125/113

IV. APPLICATION TO 6DFGS

A. Galaxy and void samples

The 6dF Galaxy Survey was undertaken with the multifiber instrument on the UK Schmidt Telescope between 2001 and 2006. The median redshift of the survey is $z = 0.052$ and it covers nearly the entire southern sky. A full description of the survey can be find in refs. [17,18] including comparisons between 6dFGS, 2dFGRS and SDSS. In this analysis we utilized the same K-band selected 6dFGS sub sample, consisting of ~70 500 galaxies, as constructed for the analysis of the baryon acoustic peak in Ref. [50]. We also used random catalogues following the same angular and redshift selection as the data sample, generated in Ref. [50].

We constructed different 6dFGS subsamples for analyzing the galaxy-galaxy and void-galaxy correlation functions. For the measurement of the void-galaxy correlation function, we first constructed a volume-limited catalogue corresponding to an approximately constant number density. This step is crucial in order to apply our measurement of the 1D real-space void-matter correlation function in Eq. (6), and to avoid any evolution in the void properties with redshift. We built the volume-limited catalogue by determining the absolute magnitude M of each galaxy using

$$m - M = 5 \log_{10} D_L(z) + 25 + K(z), \qquad (15)$$

where m is the apparent K-band magnitude, $D_L(z)$ is the luminosity distance in Mpc and $K(z)$ is the K correction

[55,56]. For this analysis we set the maximum redshift of the sample to $z_{\max} = 0.05$, in order to obtain a sample with a sufficiently high number density. The faint magnitude limit of the survey is $m_{\text{faint}} = 12.75$, and we selected all galaxies brighter than M_{faint} in the redshift range $z < z_{\max}$, where M_{faint} is computed from Eq. (15) with $z = z_{\max}$. We identified voids in the catalogue using the algorithm described in Sec. III, leading to the identification of ∼1400 voids.

B. Measurement of the correlation function

We transformed the angular coordinates and redshifts of the galaxies to comoving Cartesian coordinates assuming the same fiducial cosmology as our mock catalogue ($\Omega_m = 0.26$), although we note that the Alcock-Paczynski effect is negligible at low redshift. The separation of two galaxies along the line of sight π and across the line of sight σ is measured in the same manner as Mocks B using

$$\pi = \frac{\|\mathbf{s}.\mathbf{h}\|}{\|\mathbf{s}\|},$$
$$\sigma = \sqrt{\|\mathbf{h}\|^2 - \pi^2}, \tag{16}$$

where $\mathbf{h} = \mathbf{s_1} - \mathbf{s_2}$ is the separation of the galaxies in redshift space and $\mathbf{s} = (\mathbf{s_1} + \mathbf{s_2})/2$ is the mean distance to the galaxy pair.

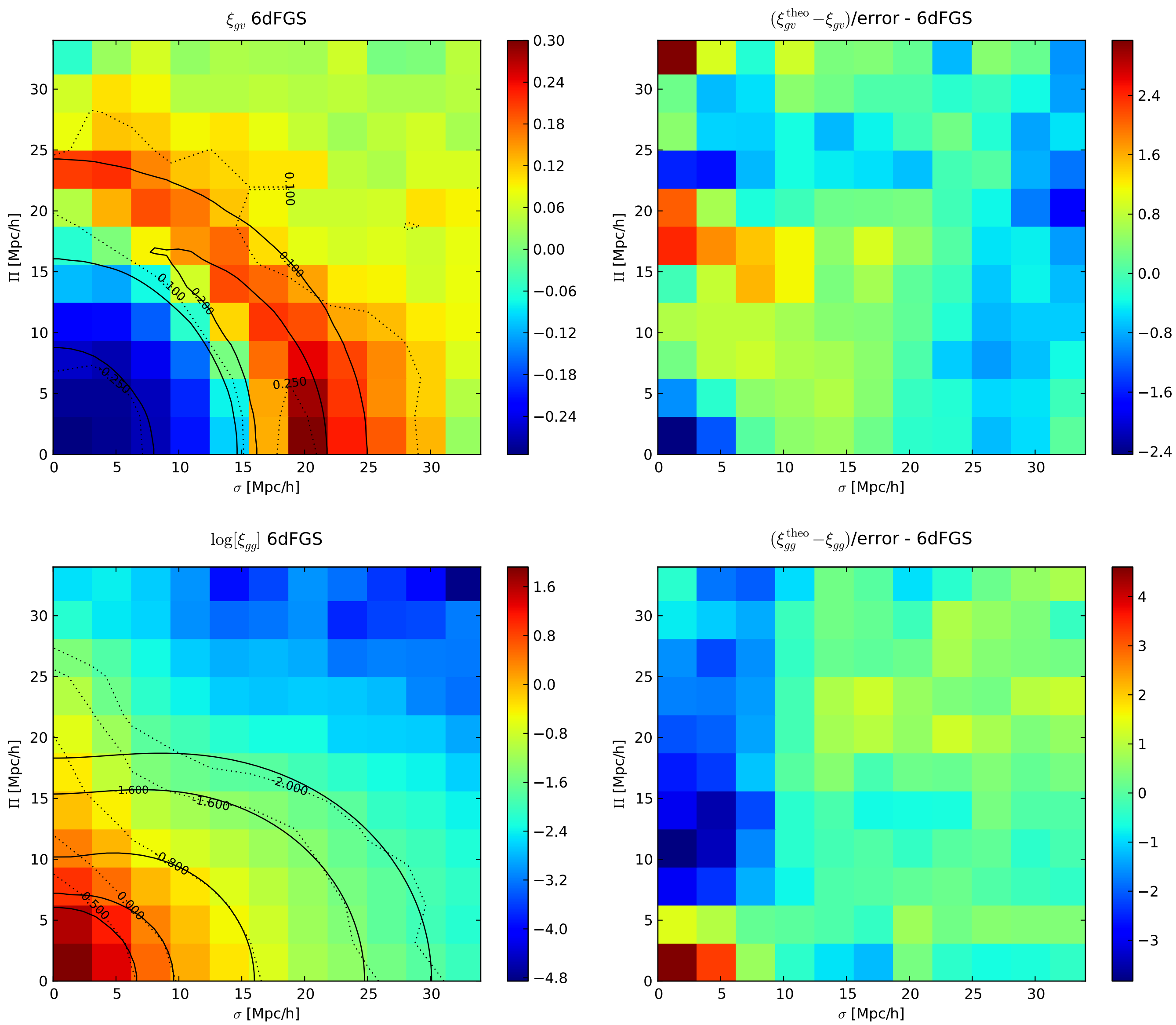

FIG. 3. The 2D void-galaxy correlation function (upper left panel) and galaxy-galaxy correlation function (lower left panel) of the 6dFGS data set. The solid lines show the best-fitting model assuming a Gaussian pairwise velocity dispersion, and the dotted lines show isocontours of the data, noting that the fitting region for the galaxy-galaxy correlation function is $\sigma > 7.5\ h^{-1}$ Mpc. The right-hand panels show the corresponding residual between the measurement and best-fitting model, scaled by the error in each bin. In general, there are not significant residuals within the fitted region.

TABLE III. Parameter constraints obtained from fitting to the 6dFGS 2D galaxy-galaxy correlation function ξ_{gg} and void-galaxy correlation function ξ_{vg}, assuming Lorentzian (L) and Gaussian (G) models for the pairwise velocity dispersion. We determine the parameter errors using the standard deviation of the parameter fits to individual mocks.

	$b\sigma_8$	$\sigma_{\rm IM}$	$f\sigma_8$	$\sigma_{\rm IM}$	σ_v[km.s^{-1}]	$\sigma_{\rm IM}$	χ^2/d.o.f
ξ_{gg} L	1.17	±0.06	0.43	±0.06	273	±92	114/192
ξ_{vg} L	0.76	±0.05	0.36	±0.11	390	±43	530/289
ξ_{gg} G	1.17	±0.06	0.42	±0.06	261	±113	116/192
ξ_{vg} G	0.80	±0.05	0.43	±0.12	515	±46	536/289

Figure 3 displays the measured 2D galaxy-galaxy correlation function (lower left) and void-galaxy correlation function (lower right) for the 6dFGS data set. For the galaxy-galaxy correlation function, we can see the elongation at small scales along the line of sight (FoG), due to the random motion of galaxies within halos. On larger scales, we observe the Kaiser effect due to coherent bulk flows. For the void-galaxy correlation function, we can detect an apparent asymmetry within the void (<15 h^{-1} Mpc): the "emptiness" is larger along the line of sight due to the cosmic expansion, and the ridge of the void (~20 h^{-1} Mpc) tends to be erased due to the velocity dispersion. The Kaiser effect can also be observed: the signal is enhanced across the line of sight, especially on the ridge.

We obtained the error in the 6dFGS void-galaxy and galaxy-galaxy correlation functions using the dispersion in the measurements from Mocks A and B, respectively. We scaled the standard deviation of the void-galaxy mock measurements to allow for the slightly different volumes of Mock A and the real data set:

$$\Delta\xi = \sqrt{\frac{V_{\rm mock}}{V_{\rm 6dFGS\text{-}cut}}} \times \sigma_{\rm mock} \tag{17}$$

where $V_{\rm 6dFGS\text{-}cut} \sim 179^3 h^{-3}$ Mpc^3 and the scaling factor is 0.64. The parameter errors are also scaled by this correction factor. No volume scaling is needed for the galaxy-galaxy correlation functions, since Mocks B sample the exact survey selection function.

C. Growth rate measurement in different environments

We fitted our RSD model to the 6dFGS data using the MCMC pipeline described in Sec. III. As previously discussed, we obtain robust parameter errors using the dispersion of the fits to the mock catalogues.

We report the best-fitting parameter values and their errors in Table III. Our measurement of the growth rate for the average of models L and G is $f\sigma_8 = 0.42 \pm 0.06$ for the galaxy-galaxy RSD and $f\sigma_8 = 0.39 \pm 0.11$ for the void-galaxy RSD. We observe larger uncertainties in the growth rate measured using the void-galaxy correlation function, although the two measurements are consistent within the statistical errors. The minimum χ^2 values, also listed in Table III, are lower than those found for the more accurate mock mean data set, but we note that they are still impacted

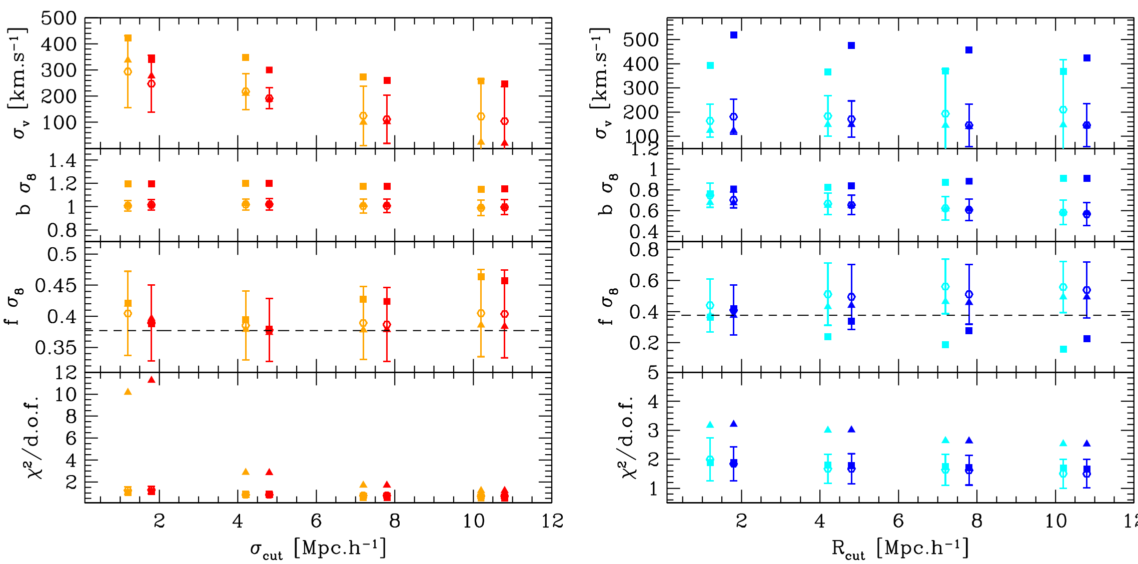

(a) Galaxy-galaxy fits as a function of the cutting scale (b) Void-galaxy fits as a function of the cutting scale

FIG. 4. The influence of the fitting range on parameter fits to the galaxy-galaxy (left panel) and void-galaxy (right panel) correlation functions. In both cases we show the result using the Gaussian pairwise velocity model (blue and red) and the Lorentzian model (orange and light blue). The squares correspond to the 6dFGS constraints, the triangles correspond to the fits to the mock mean, and the open circles correspond to the mean of the fits to individual mocks, with the error bars as the standard deviation. We offset points along the x axis for clarity.

by the assumption of a diagonal covariance matrix. The right-hand panels of Fig. 3 show the residuals between the data and best-fitting models. Our measurement is in very good agreement with the previous 6dFGS galaxy-galaxy RSD analysis [20], which obtained $f\sigma_8 = 0.42 \pm 0.05$.

The difference in the best-fitting bias parameters for ξ_{gg} and ξ_{vg} is due to the different galaxy samples used: for the galaxy-galaxy analysis we adopt a flux-limited sample across a wider redshift range, and upweight more luminous, highly biased galaxies. The best-fitting bias values are comparable with those found in the corresponding mock catalogue analyses in each case, although some differences remain.

These results are obtained with a cut $\sigma_{\rm cut} = 7.5\ h^{-1}$ Mpc for the galaxy-galaxy correlation function, and using all bins for the void-galaxy correlation function. This is motivated by the mock-catalogue analysis and the lack of sensitivity of our best-fitting parameters to these choices, which is illustrated in Fig. 4. For $\sigma_{\rm cut} > 4.5\ h^{-1}$ Mpc, the goodness-of-fit and best-fitting parameters do not significantly change for the galaxy-galaxy correlation function (left panel), independently of the model (see the red/orange solid lines). The best-fitting χ^2 of the void-galaxy correlation function (right panel) remains unchanged at all scales, independently of the model (see the blue/light blue solid lines).

Overall, the growth rate measurements are consistent between the void-galaxy and galaxy-galaxy RSD. One might think about combining these measurements to improve the uncertainties. However we do not expect a significant improvement since the growth uncertainties from the void-galaxy RSD are double those of the galaxy-galaxy RSD, and the measurements are correlated. Hence, the novelty of our result relies on the comparison of the growth between different environments.

V. CONCLUSION

In this work we provided the first direct comparison of the cosmic growth rate measured in two different environments of the same galaxy survey, by fitting to redshift space distortion in the galaxy-galaxy and void-galaxy correlation functions of the 6-degree Field Galaxy Survey. As a low-redshift survey, our 6dFGS measurements are particularly relevant for probing the late-time domination of dark energy, and are insensitive to the Alcock-Paczynski effect. We found voids using a new void-finder which identifies underdensities matching supplied density profile criteria [16]. We also note that our measurement of the growth using RSD around voids is the first performed at low redshift and in the southern hemisphere.

We determined similar growth rate measurements around galaxies ($f\sigma_8 = 0.42 \pm 0.06$) and $\sim 20\ h^{-1}$ Mpc underdensities ($f\sigma_8 = 0.39 \pm 0.11$), finding no evidence of an environmental dependence of gravitational physics. We validated our models, and estimated the errors in our measurements, using mock galaxy catalogues. Extracting the complementary cosmological information present in different environments [57,58] will be a powerful test of physics for both current galaxy redshift surveys and future projects such as Euclid [40].

Our analysis could be extended in several ways: direct measurements of peculiar velocities using standard-candle indicators could further constrain their radial profile around voids; combining our results with analyses of other data sets such as SDSS [59] and GAMA [60] can probe these effects as a function of redshift; and a comparison of our measurements with the predictions of nonstandard cosmological models, in particular modified gravity and interacting dark energy models, would place new constraints on those frameworks.

ACKNOWLEDGMENTS

We are very grateful to Yann Rasera for facilitating the access to the DEUS N-body simulations. The 6dF Galaxy Survey was made possible by contributions from many individuals towards the instrument, the survey and its science. We particularly thank Matthew Colless, Heath Jones, Will Saunders, Fred Watson, Quentin Parker, Mike Read, Lachlan Campbell, Chris Springob, Christina Magoulas, John Lucey, Jeremy Mould, and Tom Jarrett, as well as the dedicated staff of the Australian Astronomical Observatory and other members of the 6dFGS team over the years. Part of this research was conducted by the Australian Research Council Centre of Excellence for All-sky Astrophysics (CAASTRO), through project number CE110001020. We also acknowledge support from the Domaine d'intérêt majeur en astrophysique et conditions d'apparition de la vie (DIM ACAV) of the Region Ile-de-France.

[1] P. J. E. Peebles, *Principles of Physical Cosmology* (Princeton University Press, Princeton, NJ, 1993).
[2] J. Gleyzes, D. Langlois, M. Mancarella, and F. Vernizzi, J. Cosmol. Astropart. Phys. 02 (2016) 056.
[3] S. Dutta and I. Maor, Phys. Rev. D **75**, 063507 (2007).
[4] W. Hu and I. Sawicki, Phys. Rev. D **76**, 064004 (2007).
[5] J. Khoury and A. Weltman, Phys. Rev. D **69**, 044026 (2004).
[6] Y.-C. Cai, A. Taylor, J. A. Peacock, and N. Padilla, Mon. Not. R. Astron. Soc. **462**, 2465 (2016).
[7] N. Hamaus, A. Pisani, P. M. Sutter, G. Lavaux, S. Escoffier, B. D. Wandelt, and J. Weller, Phys. Rev. Lett. **117**, 091302 (2016).

[8] R. K. Sachs and A. M. Wolfe, Astrophys. J. **147**, 73 (1967).
[9] B. R. Granett, M. C. Neyrinck, and I. Szapudi, Astrophys. J. Lett. **683**, L99 (2008).
[10] C. Alcock and B. Paczynski, Nature (London) **281**, 358 (1979).
[11] G. Lavaux and B. D. Wandelt, Astrophys. J. **754**, 109 (2012).
[12] I. Achitouv, M. Neyrinck, and A. Paranjape, Mon. Not. R. Astron. Soc. **451**, 3964 (2015).
[13] I. Achitouv, M. Baldi, E. Puchwein, and J. Weller, Phys. Rev. D **93**, 103522 (2016).
[14] J. Clampitt, Y.-C. Cai, and B. Li, Mon. Not. R. Astron. Soc. **431**, 749 (2013).
[15] P. Zivick, P. M. Sutter, B. D. Wandelt, B. Li, and T. Y. Lam, Mon. Not. R. Astron. Soc. **451**, 4215 (2015).
[16] I. Achitouv, Phys. Rev. D **94**, 103524 (2016).
[17] D. H. Jones *et al.*, Mon. Not. R. Astron. Soc. **355**, 747 (2004).
[18] D. H. Jones, B. A. Peterson, M. Colless, and W. Saunders, Mon. Not. R. Astron. Soc. **369**, 25 (2006).
[19] C. Springob *et al.*, Mon. Not. R. Astron. Soc. **445**, 2677 (2014).
[20] F. Beutler, C. Blake, M. Colless, D. H. Jones, L. Staveley-Smith, G. B. Poole, L. Campbell, Q. Parker, W. Saunders, and F. Watson, Mon. Not. R. Astron. Soc. **423**, 3430 (2012).
[21] J. A. Peacock *et al.*, Nature (London) **410**, 169 (2001).
[22] E. Hawkins *et al.*, Mon. Not. R. Astron. Soc. **346**, 78 (2003).
[23] S. Cole *et al.*, Mon. Not. R. Astron. Soc. **362**, 505 (2005).
[24] M. Tegmark, Phys. Rev. Lett. **79**, 3806 (1997).
[25] C. Blake *et al.*, Mon. Not. R. Astron. Soc. **425**, 405 (2012).
[26] B. Reid *et al.*, Mon. Not. R. Astron. Soc. **426**, 2719 (2012).
[27] B. A. Reid, H.-J. Seo, A. Leauthaud, J. L. Tinker, and M. White, Mon. Not. R. Astron. Soc. **444**, 476 (2014).
[28] F. Beutler *et al.*, Mon. Not. R. Astron. Soc. **443**, 1065 (2014).
[29] S. de la Torre *et al.*, Astron. Astrophys. **557**, A54 (2013).
[30] P. A. R. Ade *et al.* (Planck Collaboration), Astron. Astrophys. **594**, A13 (2016).
[31] A. J. Hawken *et al.*, arXiv:1611.07046.
[32] N. Kaiser, Mon. Not. R. Astron. Soc. **227**, 1 (1987).
[33] A. J. S. Hamilton, P. Kumar, E. Lu, and A. Matthews, Astrophys. J. Lett. **374**, L1 (1991).
[34] A. Lewis and S. Bridle, Astrophysics Source Code Library, record ascl:1106.025.
[35] E. Komatsu *et al.*, Astrophys. J. Suppl. Ser. **180**, 330 (2009).
[36] N. Hamaus, P. M. Sutter, G. Lavaux, and B. D. Wandelt, J. Cosmol. Astropart. Phys. 11 (2015) 036.
[37] M. Kopp, C. Uhlemann, and I. Achitouv, Phys. Rev. D **94**, 123522 (2016).
[38] T. Hamana, I. Kayo, N. Yoshida, Y. Suto, and Y. P. Jing, Mon. Not. R. Astron. Soc. **343**, 1312 (2003).
[39] V. Desjacques, D. Jeong, and F. Schmidt, arXiv:1611.09787.
[40] http://www.euclid-ec.org/.
[41] J. Courtin, Y. Rasera, J.-M. Alimi, P.-S. Corasaniti, V. Boucher, and A. Fzfa, Mon. Not. R. Astron. Soc. **410**, 1911 (2011).
[42] J.-M. Alimi, A. Fzfa, V. Boucher, Y. Rasera, J. Courtin, and P.-S. Corasaniti, Mon. Not. R. Astron. Soc. **401**, 775 (2010).
[43] Y. Rasera *et al.*, Mon. Not. R. Astron. Soc. **440**, 1420 (2014).
[44] I. Achitouv, C. Wagner, J. Weller, and Y. Rasera, J. Cosmol. Astropart. Phys. 10 (2014) 077.
[45] R. Teyssier, Astron. Astrophys. **385**, 337 (2002).
[46] T. Baldauf, U. Seljak, R. E. Smith, N. Hamaus, and V. Desjacques, Phys. Rev. D **88**, 083507 (2013).
[47] J. Koda, C. Blake, F. Beutler, E. Kazin, and F. Marin, Mon. Not. R. Astron. Soc. **459**, 2118 (2016).
[48] F. Beutler, C. Blake, J. Koda, F. Marin, H.-J. Seo, A. Cuesta, and D. Schneider, Mon. Not. R. Astron. Soc. **455**, 3230 (2016).
[49] F. Beutler *et al.*, Mon. Not. R. Astron. Soc. **429**, 3604 (2013).
[50] F. Beutler, C. Blake, M. Colless, D. H. Jones, L. Staveley-Smith, L. Campbell, Q. Parker, W. Saunders, and F. Watson, Mon. Not. R. Astron. Soc. **416**, 3017 (2011).
[51] P. Carter *et al.* (to be published).
[52] N. Hamaus, B. D. Wandelt, P. M. Sutter, G. Lavaux, and M. S. Warren, Phys. Rev. Lett. **112**, 041304 (2014).
[53] H. A. Feldman, N. Kaiser, and J. A. Peacock, Astrophys. J. **426**, 23 (1994).
[54] http://www.getdist.readthedocs.io/en/latest/.
[55] D. W. Hogg, I. K. Baldry, M. R. Blanton, and D. J. Eisenstein, arXiv:astro-ph/0210394.
[56] F. Mannucci, F. Basile, B. M. Poggianti, A. Cimatti, E. Daddi, L. Pozzetti, and L. Vanzi, Mon. Not. R. Astron. Soc. **326**, 745 (2001).
[57] I. Achitouv and C. Blake, Phys. Rev. D **92**, 083523 (2015).
[58] F.-S. Kitaura *et al.*, arXiv:1511.4405.
[59] http://www.sdss.org/.
[60] http://www.gama-survey.org/.